Naval Research Laboratory

Washington, DC 20375-5320

NRL/MR/5670--98-8186

Preliminary Results on the Monitoring of an In-Service Bridge Using a 32-Channel Fiber Bragg Grating Sensor System

S. T. VOHRA

Fiber Optic Smart Structure Group
Optical Sciences Division

C . C. CHANG
B. ALTHOUSE

URF, Greenbelt, MD

B. A. DANVER

SFA Inc., Largo, MD

M. A. DAVIS

CiDRA Corporation, Wallingford, CT

R. IDRISS

New Mexico State University, Las Cruces NM

July 10, 1998

REPORT DOCUMENTATION PAGE

Form Approved
OMB No. 0704-0188

1. AGENCY USE ONLY (*Leave Blank*)	2. REPORT DATE	3. REPORT TYPE AND DATES COVERED
	July 10, 1998	

4. TITLE AND SUBTITLE

Preliminary Results on the Monitoring of an In-Service Bridge Using a 32-Channel Fiber Bragg Grating Sensor System

5. FUNDING NUMBERS

6. AUTHOR(S)

S.T. Vohra, C.C. Chang,* B.A. Danver,† B. Althouse,* M.A. Davis,‡ and R. Idriss**

7. PERFORMING ORGANIZATION NAME(S) AND ADDRESS(ES)

Naval Research Laboratory
Washington, DC 20375-5320

8. PERFORMING ORGANIZATION REPORT NUMBER

NRL/MR/5670--98-8186

9. SPONSORING/MONITORING AGENCY NAME(S) AND ADDRESS(ES)

DOT

10. SPONSORING/MONITORING AGENCY REPORT NUMBER

11. SUPPLEMENTARY NOTES

*URF, 6411 Ivy Lane, Suite 110, Greenbelt, MD 20770
†SFA Inc., 1401 McCormick Dr., Largo, MD 20770
‡CiDRA Corp., 15 Sterling Dr., Wallingford, CT 06492
**New Mexico State University, Las Cruces, NM 88003

12a. DISTRIBUTION/AVAILABILITY STATEMENT

Approved for public release; distribution unlimited.

12b. DISTRIBUTION CODE

A

13. ABSTRACT (*Maximum 200 words*)

This report describes the preliminary results of the performance of a 32-channel fiber Bragg grating (FBG) system used to monitor the dynamic response of an in-service interstate bridge (North-bound span, I-10 at University Blvd., Las Cruces, New Mexico). Fiber Bragg grating sensors were attached on four different support girders in groups of three at various locations along the span of the bridge. Using an interrogation approach based on the scanning Fabry-Perot system, the sensors were monitored for various vehicle loading conditions. They dynamic response of the bridge to a typical traffic load event as detected by a group of three sensors on a particular girder is illustrated in some detail by describing the data both in time and frequency domains. This is followed by a description of the response of all 32 sensors on the bridge to two traffic loading events. The field test results indicate that the natural resonant frequencies of the first two longitudinal modes of the bridge are ~2.5 Hz and ~3.8 Hz, respectively. The preliminary results reported here clearly demonstrate that an optical FBG sensor system is ideally suited for monitoring weigh-in-motion traffic events as well as for providing the dynamic properties of bridge structures.

14. SUBJECT TERMS

Fiber optic sensors

15. NUMBER OF PAGES

24

16. PRICE CODE

17. SECURITY CLASSIFICATION OF REPORT	18. SECURITY CLASSIFICATION OF THIS PAGE	19. SECURITY CLASSIFICATION OF ABSTRACT	20. LIMITATION OF ABSTRACT
UNCLASSIFIED	UNCLASSIFIED	UNCLASSIFIED	UL

NSN 7540-01-280-5500

Standard Form 298 (Rev. 2-89)
Prescribed by ANSI Std 239-18
298-102

CONTENTS

PRELIMINARY RESULTS ON THE MONITORING OF AN IN-SERVICE BRIDGE USING A 32-CHANNEL FIBER BRAGG GRATING SENSOR SYSTEM

ABSTRACT

Design and performance of a 32-channel fiber Bragg grating (FBG) system used to monitor the dynamic response of an in-service interstate bridge[5] are reported. Fiber Bragg grating sensors were attached on four different support girders in groups of three at various locations along the span of the bridge. Using an interrogation approach based on the scanning Fabry-Perot system, the FBG sensors were monitored for various vehicle loading conditions. The response of the bridge to a typical traffic loading is described both in time and frequency domains. The preliminary results of the field test reported here clearly demonstrate that an optical FBG sensor system is well suited for monitoring both, weigh-in-motion traffic events as well as the dynamic characteristics of bridge structures.

INTRODUCTION

Fiber optic sensors have been proposed for use in numerous field applications, such as evaluation of strains and stresses in structures. Fiber optic sensors offer a series of unique advantages over their conventional electronic counterparts including electromagnetic immunity, light weight, small size, low transmission loss, and resistance to corrosion. Fiber Bragg grating (FBG) sensors are particularly attractive for distributed structural sensing since they offer wavelength encoded operation. FBGs are wavelength-encoded in that the strain information obtained from the device is contained within the reflected wavelength components. Another major advantage of wavelength encoded operation is that it simplifies the process of multiplexing numbers of FBG sensors on a single strand of optical fiber. The multiplexed devices can be written at different initial spectral locations that can be correlated to the physical location of each device along the fiber. Any wavelength shift of a given grating can be attributed to the localized strain at that particular location and a quasi-distributed strain sensor system can be created with a minimum of optical fibers. Much of the recent work in the field has focused on the development of a variety of wavelength detection techniques which provide the capability to

[5]North-bound span, I-10 at University Blvd., Las Cruces, New Mexico

Manuscript approved March 23, 1998.

demodulate and multiplex several FBG strain sensors using either the inherent wavelength division addressing capabilities of FBGs or by a using a hybrid wavelength-time division multiplexing approach [1]. This report describes the results of field test carried out using a wavelength division multiplexed array of 32 FBGs attached at various locations along the girders of an in-service bridge in New Mexico. The FBG responses are interrogated using a method based on the scanning fiber Fabry-Perot (FFP) filter [2]. Preliminary data obtained from the 32 FBGs indicates that the magnitude of the dynamic strains induced in the bridge by moving vehicles is under 1000 με and the frequencies excited in the structure are well below 20 Hz.

FBG INTERROGATION SYSTEM

One of the more successful techniques for interrogating FBG sensors involves the use of tunable passband Fabry-Perot (FP) filter for tracking the FBG signal [2]. In this approach, light reflected back from an array of Bragg grating sensors is passed through a FP filter which passes one narrowband wavelength, depending on the spacing between the mirrors in the device. The narrowband wavelength signal is passed on to the photodetector and electronically differentiated. This produces a series of pulses for each of the signal reflected by the FBGs with the zero-crossing of each pulse representing the peak reflected wavelength from each sensor. The zero-crossings are recorded by a computer along with the digital value of the ramp voltage applied to the FP system. By referencing any shifts in the zero-crossings from each FBG to the voltage applied to the FP filter, the strain in each FBG sensor can be obtained. The schematic of the electro-optical system used in this study is shown in Figure 1. The free spectral range (FSR) and the resolution bandwidth along with the spectral spacing between the FBGs determine the number of FBG sensors which can be interrogated per one scan of the FP filter. The choice of 16 bit resolution for the FP ramp, and a FSR of 45 nm produces a minimum detectable wavelength shift of 0.7 pm, or equivalent strain resolution of less than 1 με. However, the actual minimum detectable strain is on the order of ~5 με with consideration of noise from the electronic system. For the field test reported in this work, a scanning FP system similar to the one just described was used to interrogate 32 FBG sensors.

As shown in Figure 1, light from two ELEDs is directed through a pair of 2x2 couplers connected to two FBG sensor arrays. Each FBG array is made up of sixteen FBG sensors. The

reflected light from the FBG arrays is combined with a third coupler and directed to a single FP filter. The fiber Fabry-Perot filter used in this work had an FSR of about 45 nm, thus allowing 16 individual sensors with a bandwidth of ~0.2 nm, spaced by approximately 2.7 nm to be interrogated per filter scan. This spacing is sufficient to allow strains of about ±1300 με for each FBG to be easily monitored. The FFP filter is capable of achieving scan rates of about 360 Hz and supporting 64 FBGs but in this work the system was set to operate at a sampling rate of 45 Hz. This was driven by two reasons: (1) only the up scan was used to prevent the hystersis difference of voltage-to-wavelength tuning response between the up and down scan, and (2) the FBG sensor readings were averaged 4 times to provide better resolution. The ELEDs' on/off was synchronized with the ramp of the filter drive voltage such that only the FBG array being interrogated by the FP filter was lit at any given time. It should be pointed out that in monitoring large scale structures, static and quasi-static strains (< 10 Hz) are of prime interest and in the particular case of the structure being reported here, sampling rate of 45 Hz was considered adequate. However, by using different FP filters capable of providing higher sampling rate or by modifying the approach utilized here, it should be possible to achieve significantly enhanced sampling rates (≈ 1 kHz).

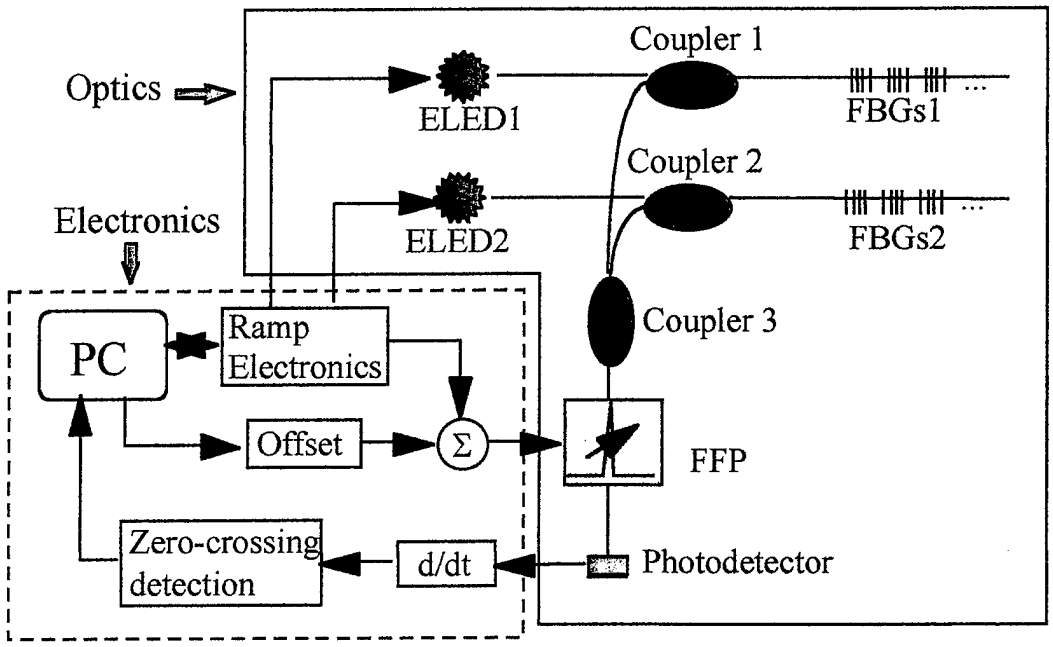

Figure 1 The schematic of the FP instrumentation system to interrogate the FBG array

SPECTRAL AND PHYSICAL ARRANGEMENT OF FBG SENSORS

The spectral characteristic of the ELED output has a Gaussian-like distribution [3]. Therefore, in order to maximize the signal-to-noise (SNR) ratio at each FBG wavelength the reflectivities of the FBGs must be tailored accordingly. In other words, the FBG reflectivities were tailored such that the high reflectivity FBGs had their Bragg wavelengths fall near the wings of the ELED spectrum while FBGs with lower reflectivities had their Bragg wavelengths fall around the center of the ELED spectrum. This ensured, approximately, equal amounts of light being reflected back from all the FBG sensors, thus resulting in reduced variation in the SNR among various FBG sensors. The FBG sensors used on the bridge had tailored reflectivities to achieve approximately equal light levels from all the sensors.

The I-10 bridge over Las Cruces, New Mexico, consists of spans made up of a concrete deck supported by welded steel plate girders (Figure 2). Each span is about 36 meters long and FBG sensors were attached at the pier, 1/8-span and 1/2-span of girder 1, girder 2, girder 3 and girder 4.

Figure 2 A photograph showing continuous girders along the span of the I-10 Bridge. A small portion of the pier is shown in the upper left corner for perspective. The girders were labeled in ascending order starting from left to right (arbitrarily). FBG sensors were placed on girders 1 to 4 at the pier, 1/8-span and 1/2-span.

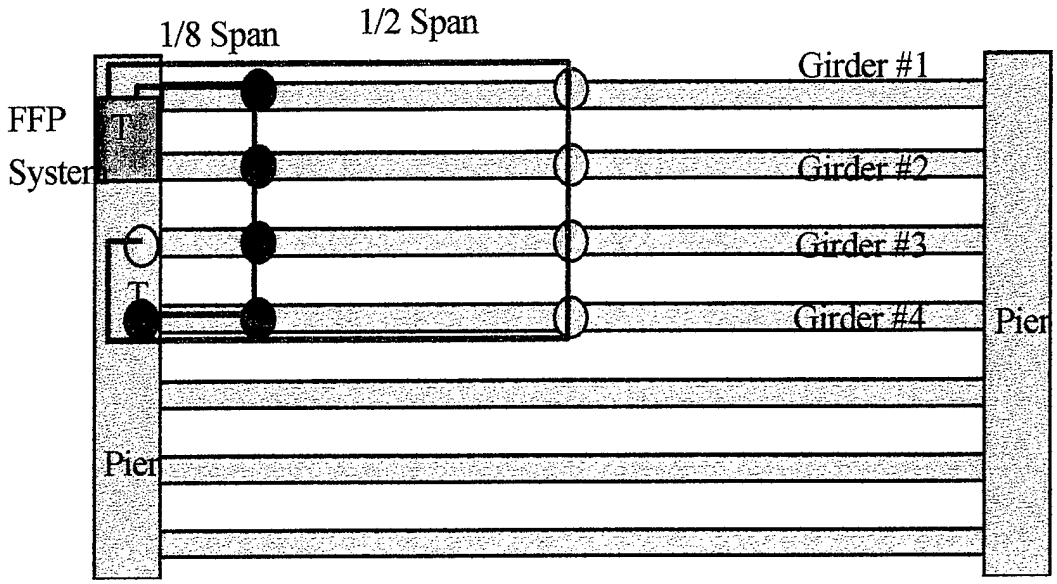

Figure 3 A schematic of the arrangement of FBG sensors on the girders as it would look from above this bridge. Sensors were attached at 1/8-span, 1-2 span and the pier. FBG sensors were only placed on girders 1 to 4. Traffic direction is from left to right in the above schematic.

A sketch indicating the sensor locations on the girders is shown in Figure 3. Three FBGs, ranging from lowest to highest wavelength in a given sub-array, are surface mounted on the top flange, upper web and bottom flange of the girder, as shown in Figure 4. In each FBG location, a small area of the girder was filed smooth and prepared by following the installation tips for the conventional resistance strain gage and the FBG were bonded using M-Bond 200 adhesive. For the first FBG array (also know as the 1/2-span array), the temperature reference sensor, T, is installed inside of the FBG instrumentation (FFP system) located on one of the piers and is used to temperature-compensate the rest of 31 FBGs.

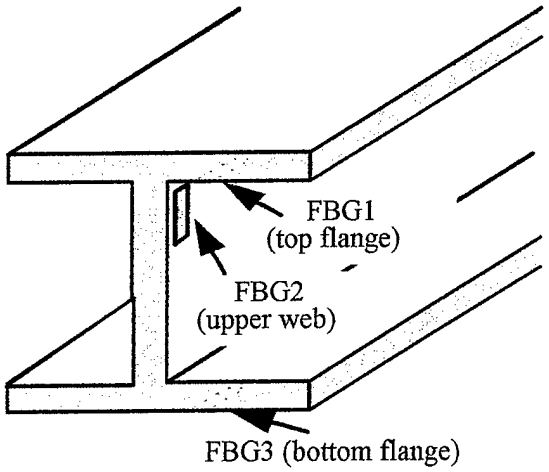

Figure 4 Local arrangement of the FBG sensors at each girder location. Sensors were placed on the top flange, the web and bottom flange of the girder.

PRELIMINARY RESULTS OF I-10 BRIDGE MONITORING

The fiber Fabry-Perot (FFP) system for interrogating the arrays was located on one of the bridge piers and is designed to have a sampling rate of 45 Hz. The data from the FBG arrays is stored onto a computer hard disk using a threshold trigger method which allows storage of data only if a certain strain threshold is crossed. In the measurements described here, the data collection software was set to store data only if a 20 με loading event is experienced at the FBG sensor located on the bottom flange of girder 3. This approach allows judicious storage of data on the computer hard drive by allowing data with significant loading events only to be stored. It should be pointed out that the FFP system is continuously monitoring the arrays but storage of the data occurs only if the strain threshold is crossed. Each data file includes 32 columns of 1350 data points (equivalent to data recorded in 30 seconds at 45 Hz sampling rate) corresponding to each FBG on the bridge. The program assigns a 225-points pre-trigger length (equivalent to 5 seconds).

The response of FBG sensors located at half-span, girder 3 of the bridge to a vehicle load event is shown in Figure 5. Data from FBG sensors located on the top flange, the web and the bottom flange are depicted in Figure 5. The data clearly shows that during a 30-seconds duration,

a large strain event (e.g. a truck) followed by a smaller strain event (e.g. a car) takes place on the bridge. All three FBG sensors located on girder 3 recorded the data as expected. The truck, seen as the large peak, produces a peak negative strain of about 40 με at the top flange location, peak negative strain of about 100 με at the web location and peak positive strain of about 80 με at the bottom flange location. Modal excitations of the bridge induced by the transient loading event can be seen (Figure 5c).

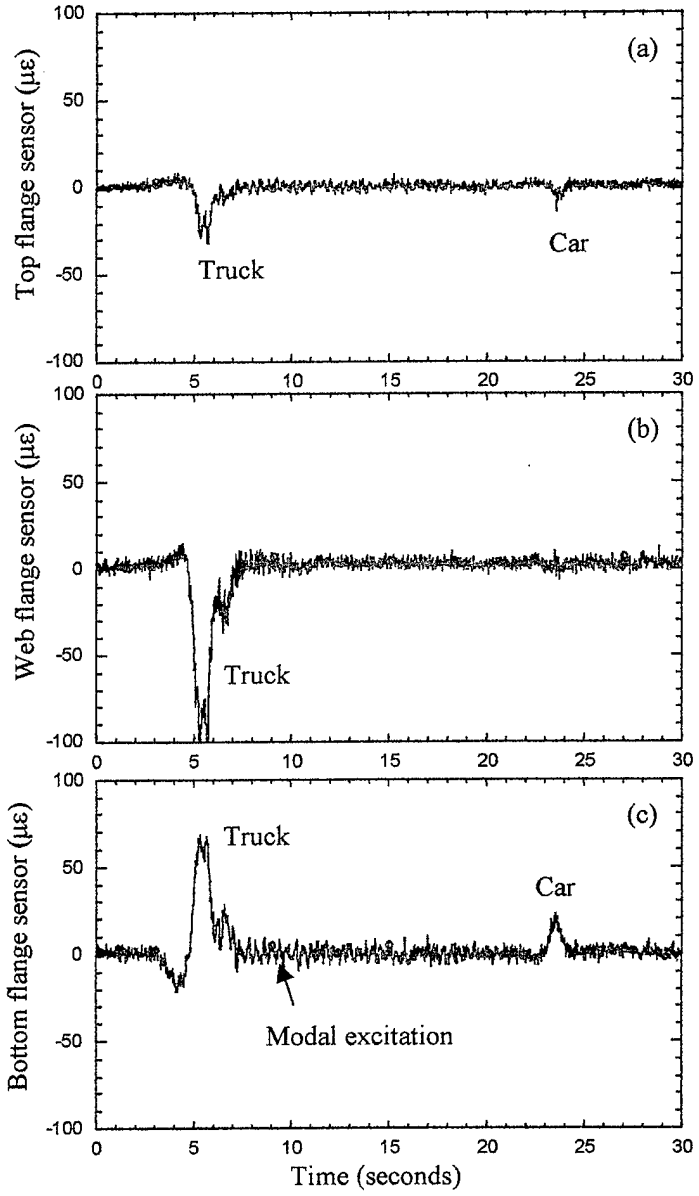

Figure 5 Responses due to transient loading from FBG sensors located at (a) the top flange, (b) the web and (c) the bottom flange of the half-span, girder 3

A closer look at the data reveals that the strain response at all three locations changes sign between the time period of 3 to 7 seconds. For instance, in Figure 5c (bottom flange FBG sensor), negative strain of about 20 με is observed in the FBG sensor followed by a sharp rise in strain towards the positive direction, eventually peaking at about 80 με. This can be explained as follows. The I-10 bridge girder is a continuous structure which undergoes compressive strain at the bottom flange prior to the truck reaching the sensor location (half-span, girder 3). The truck travelling at about 65 mph then reaches the location directly above half-span girder 3, thus inducing a bend in the beam due to direct loading which results in positive strain at the bottom flange of the I-beam. This is followed by transient load (i.e. truck) induced modal excitations in the bridge, which can be seen as ringing in the FBG sensor response (Figure 5c). A similar argument explains the top flange and web sensor responses.

Since the top flange sensor is on the opposite side of the neutral axis of the I-beam with respect to the bottom flange sensor, the sign of measured strain between the top and bottom flange is reversed for the same loading event at that location. The web sensor is located significantly closer to the top flange of the I-beam. The web sensor shows large compressive strain signal during the actual transit of the truck directly over the sensor location. This is preceded by a slight positive strain at the web sensor for the same reasons as described earlier. The second event in Figure 5, near the 23-seconds mark, can be attributed to a smaller vehicle, a car, passing over that location producing a peak strain of about 25 με. The bottom flange undergoes tension and the top flange (above the neutral axis) undergoes compression, resulting in positive and negative strains at those locations due to the vehicle. The car does not induce noticeable bridge vibrations.

Power spectral density calculations were performed on the time series data generated from the FBG sensors installed on the bridge. The time series data shown in Figure 5 was used to estimate the frequency content. Since the induced bridge vibrations are significantly smaller in magnitude than the measured strain due to a vehicle passing directly above sensor location, the spectra were computed in two parts. Figure 6a shows the power spectra of the first eight seconds of the time series obtained from the three FBG sensors (top flange, bottom flange and web) located at girder 3, half-span. The spectra of Figure 6a clearly show that a large and broad strain peak well in the sub-Hertz regime. Considering the transient nature of the event other analytical techniques (e.g. wavelet transforms) may be better suited to analyze such events in the time series. However, the power spectrum density obtained from the data for time periods beyond 8

seconds clearly show distinct peaks at 2.6 Hz and beyond (up to 8.7 Hz). The peaks observed in Figure 6b are due to various vibrational modes being excited in the bridge due to the transient loading event (i.e. due to the heavy truck passing over the bridge). No significant vibrations with frequencies above 10 Hz were observed during the period of observation reported here.

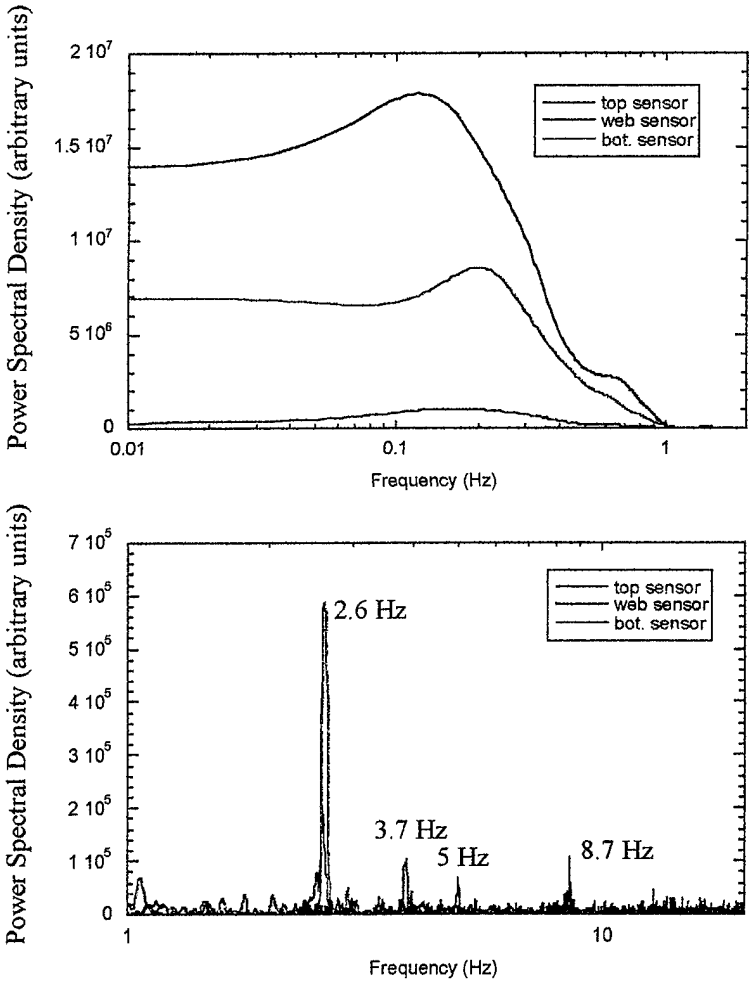

Figure 6 Power spectral density (in arbitrary amplitude units) of the top flange, bottom flange and the web FBG sensors located at girder 3, half-span (see Fig. 5 for corresponding time series). The top part of the figure, (a) shows the power spectra of the data corresponding to the first 8 seconds of the time series while (b) corresponds to the power spectra of the time series from 8 to 30 seconds.

With the same span (half-span) the strain response and power spectral density of FBGs sensors located at girders 1, 2 and 4 of the bridge to vehicle load events are shown in Figures 7 through 12. From the time traces shown in Figures 7, 9 and 11 (corresponding to girder 1, 2 and 4), the top and bottom flange sensor also indicate two dynamic events caused by the truck and car. By examining the magnitudes of FBG sensors at four girders, it seems that the truck passed over the girder 2 to cause larger bending strains and smaller torsional strain. An observation from the power spectral density (PSD) shown in Figure 6b is that the tonal vibration near 2.6 Hz was also observed in top and bottom flange sensors at girder 1, 2 and 4, particularly in bottom sensors. It indicates that the 2.6 Hz vibration measured in the bridge represents the fundamental mode of the given bridge structure. In addition, tonals at frequencies near 3.7~4.1 Hz was observed in the bottom sensors of four girders indicating a higher mode of the bridge structure. Tonals at frequencies near 5 and 8.7 Hz observed at half-span, girder 3 (Figure 6b) indicates that higher order torsional modes were excited by the traffic events.

Finally, the strain response and power spectral density of FBGs sensors located at the zero-span, 1/8 span of girder 3 of the bridge to vehicle load events are shown in Figures 13 through 16. From the time traces shown in Figures 13 and 15 (zero-span and 1/8 span), the top and bottom flange sensor responses indicate two dynamic events caused by the truck and car except for the top sensor at the zero-span. It is because the zero-span supported by abutment are less sensitive to traffic events. The time traces of flange sensors experiences opposite peak strains compared to the flange sensors at the half span. It is also due to the sensors located at or near by the nodal points of the bridge structure. An observation from the PSD in Figure 14 (zero-span) does not show any significant resonant frequency due to its physical location while the PSD in Figure 16 (1/8 span) shows a tonal frequency near 2.6 Hz. It ensures that 2.6 Hz is the resonant frequency of the fundamental mode of the bridge.

Data from all the FBG sensors located in a spatially distributed manner should allow us to determine which lanes of the bridge are most often being used, the speed of the vehicle, the load being carried by the vehicle, while the vibrational spectra obtained from the sensors should allow for determination of the modal excitations being induced in the bridge

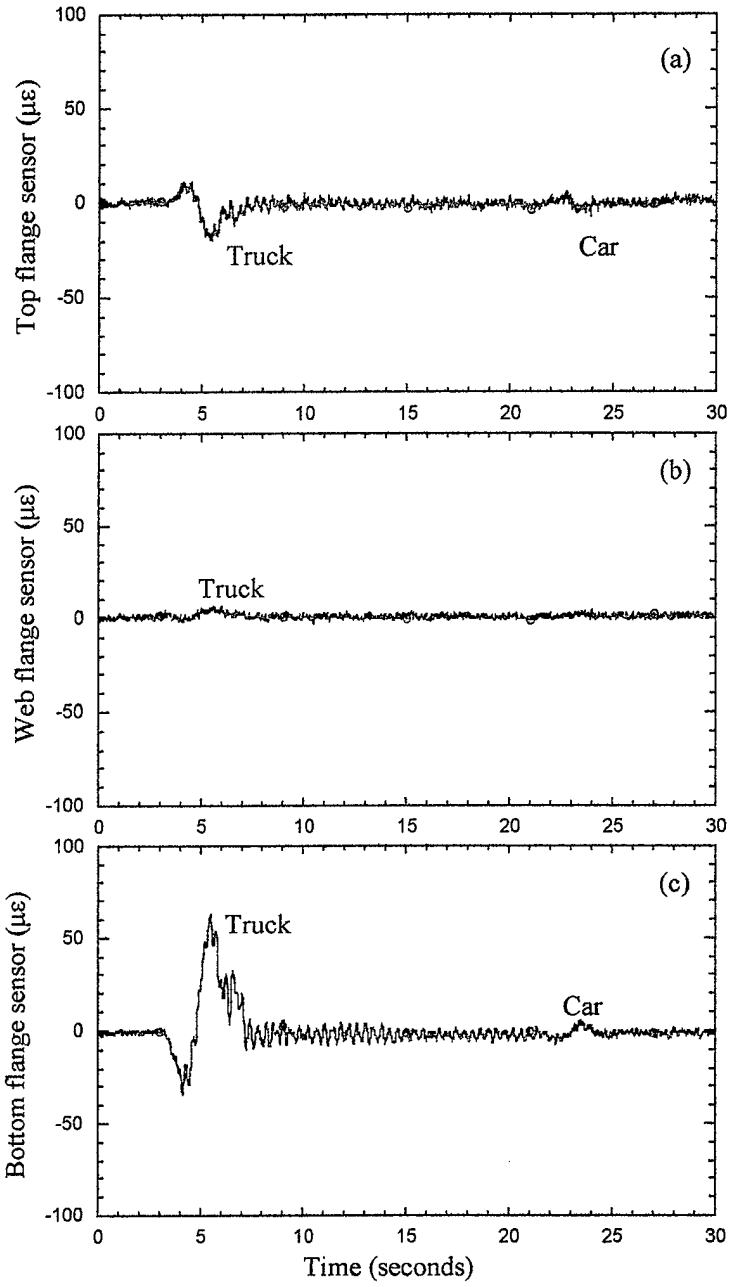

Figure 7 Responses due to transient loading from FBG sensors located at (a) the top flange, (b) the web and (c) the bottom flange of the half-span, girder 1

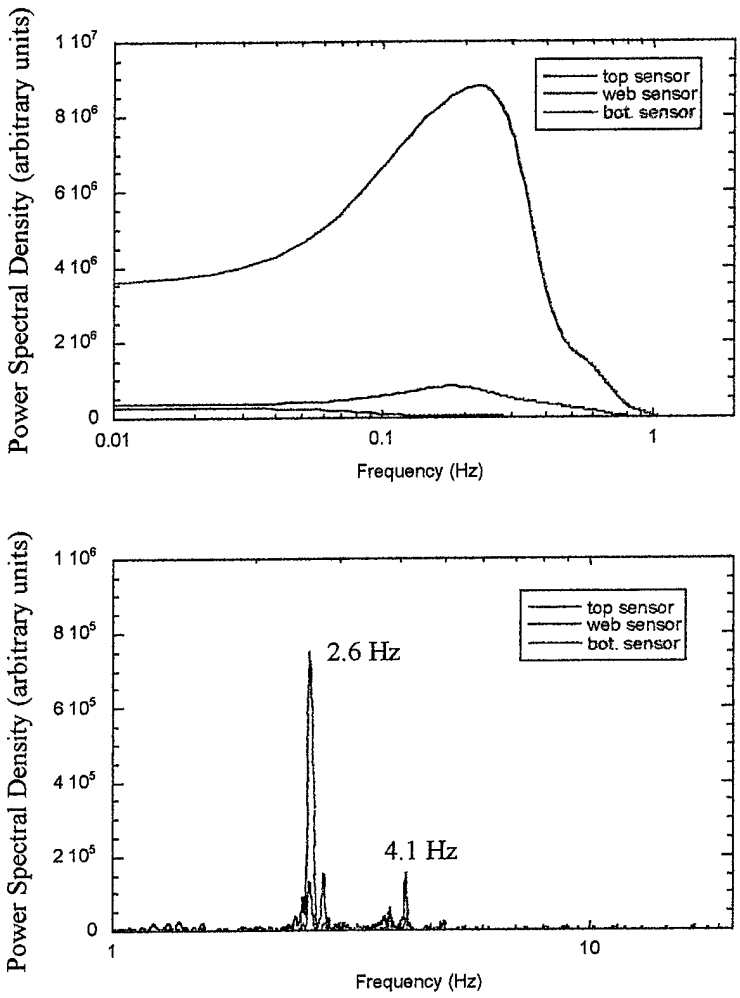

Figure 8 Power spectral density (in arbitrary amplitude units) of the top flange, bottom flange and the web FBG sensors located at girder 1, half-span (see Fig. 7 for corresponding time series). The top part of the figure, (a) shows the power spectra of the data corresponding to the first 8 seconds of the time series while (b) corresponds to the power spectra of the time series from 8 to 30 seconds.

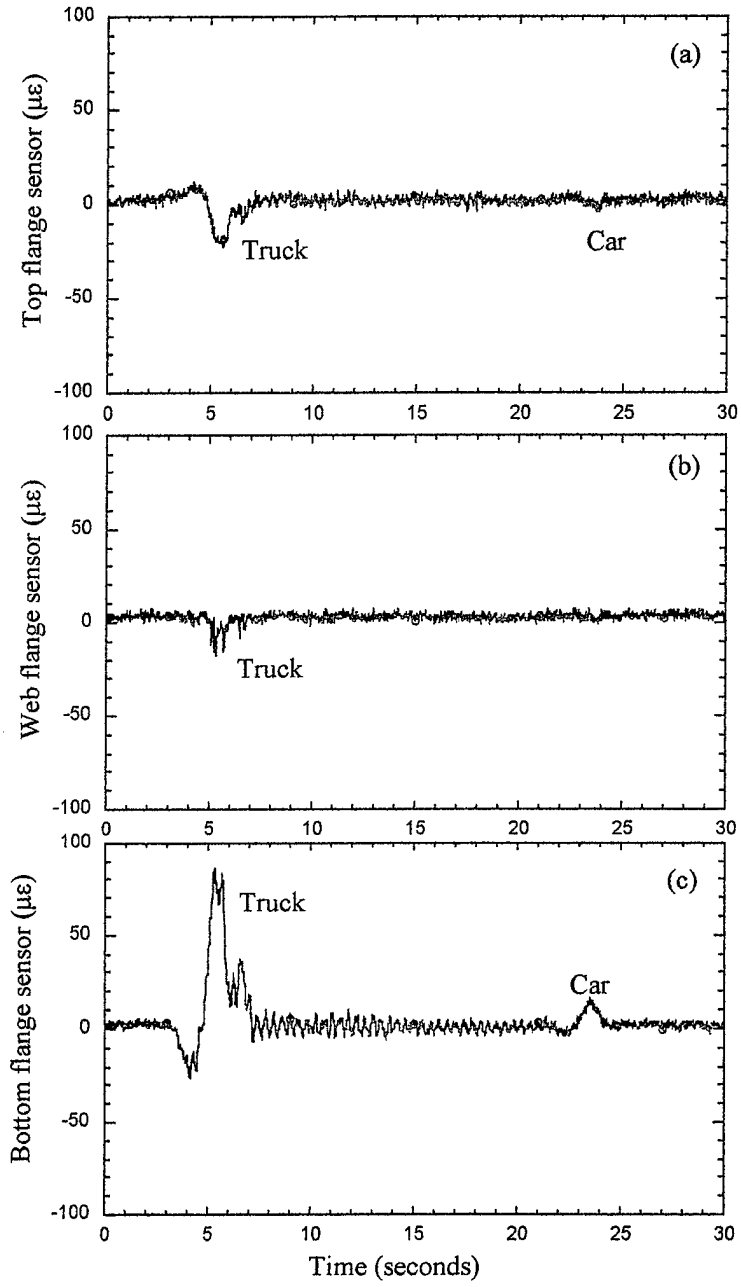

Figure 9 Responses due to transient loading from FBG sensors located at (a) the top flange, (b) the web and (c) the bottom flange of the half-span, girder 2

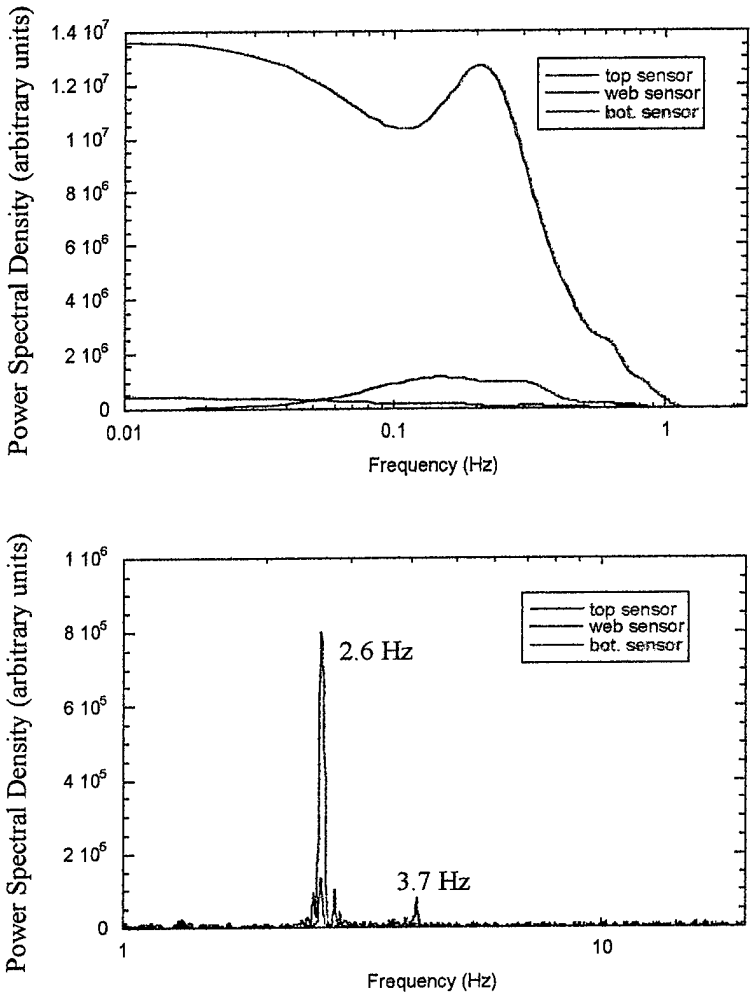

Figure 10 Power spectral density (in arbitrary amplitude units) of the top flange, bottom flange and the web FBG sensors located at girder 2, half-span (see Fig. 9 for corresponding time series). The top part of the figure, (a) shows the power spectra of the data corresponding to the first 8 seconds of the time series while (b) corresponds to the power spectra of the time series from 8 to 30 seconds.

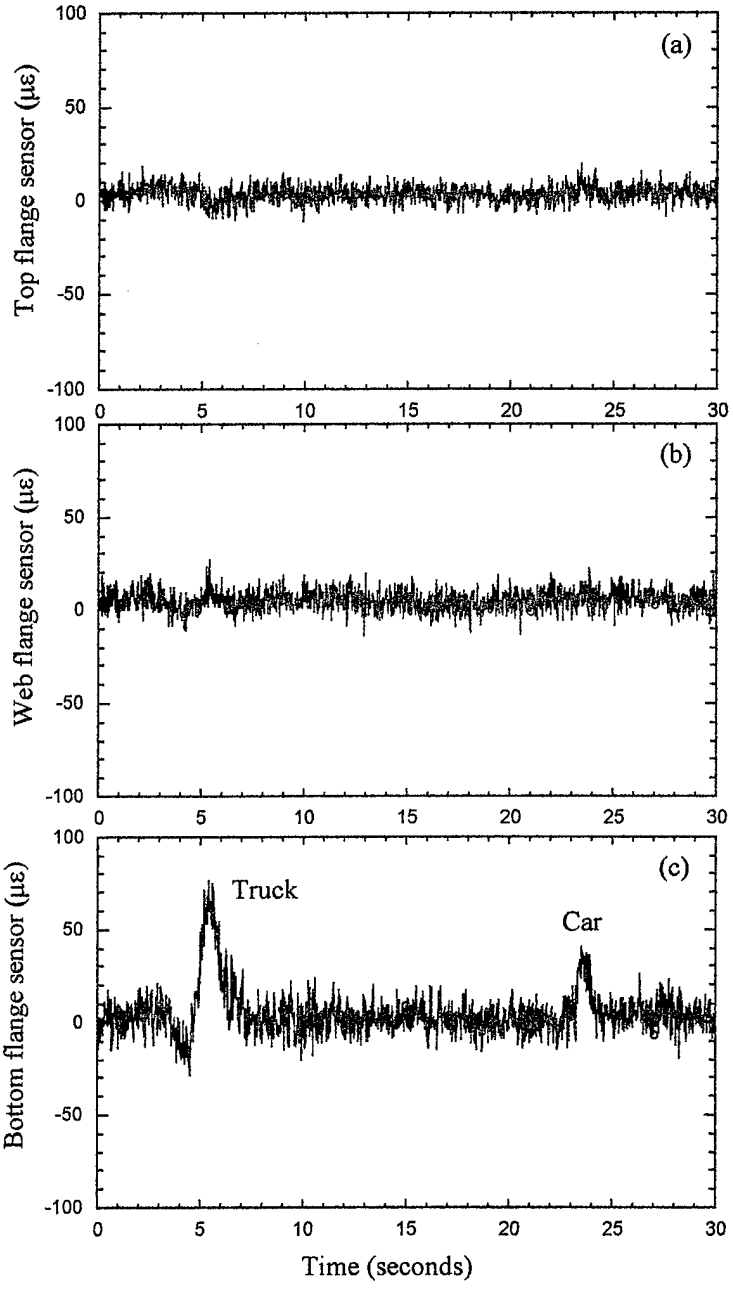

Figure 11 Responses due to transient loading from FBG sensors located at (a) the top flange, (b) the web and (c) the bottom flange of the half-span, girder 4

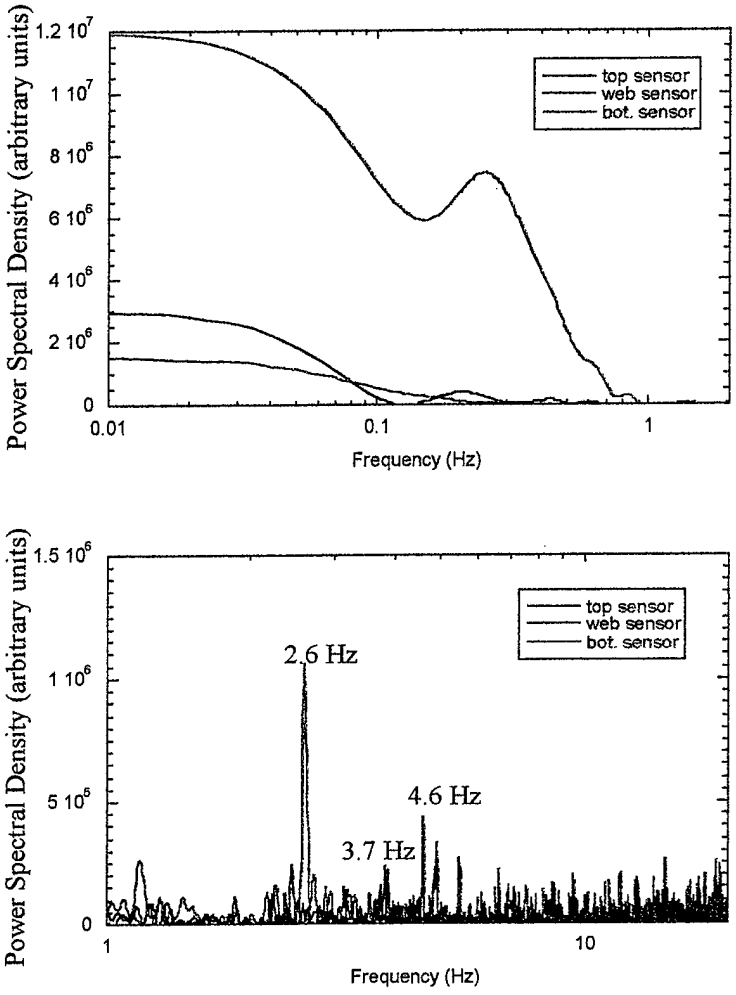

Figure 12 Power spectral density (in arbitrary amplitude units) of the top flange, bottom flange and the web FBG sensors located at girder 4, half-span (see Fig. 11 for corresponding time series). The top part of the figure, (a) shows the power spectra of the data corresponding to the first 8 seconds of the time series while (b) corresponds to the power spectra of the time series from 8 to 30 seconds.

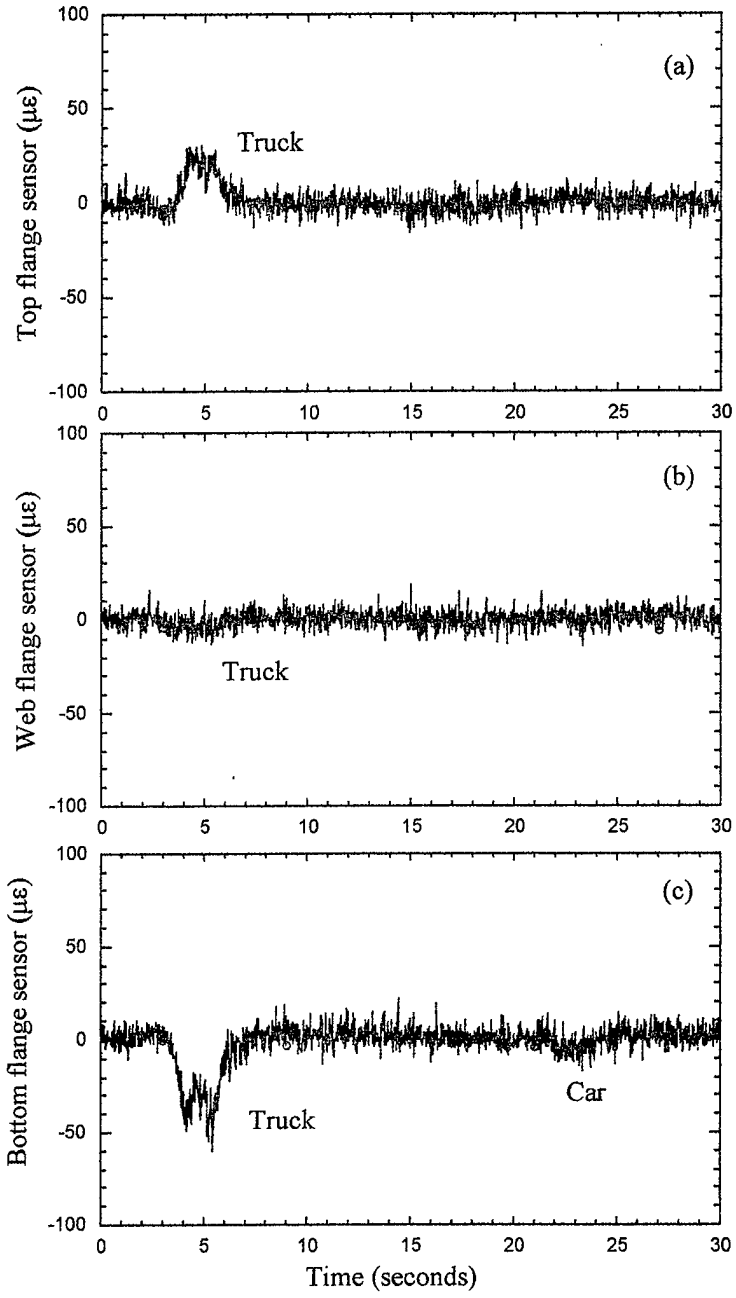

Figure 13 Responses due to transient loading from FBG sensors located at (a) the top flange, (b) the web and (c) the bottom flange of the zero-span, girder 3

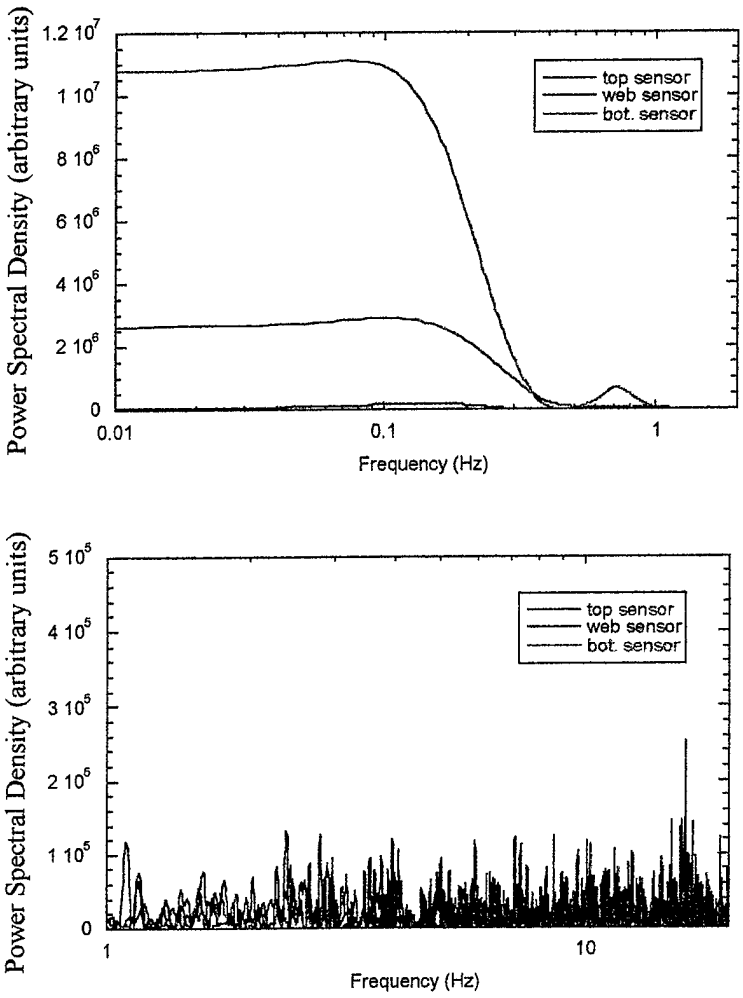

Figure 14 Power spectral density (in arbitrary amplitude units) of the top flange, bottom flange and the web FBG sensors located at girder 3, zero-span (see Fig. 13 for corresponding time series). The top part of the figure, (a) shows the power spectra of the data corresponding to the first 8 seconds of the time series while (b) corresponds to the power spectra of the time series from 8 to 30 seconds.

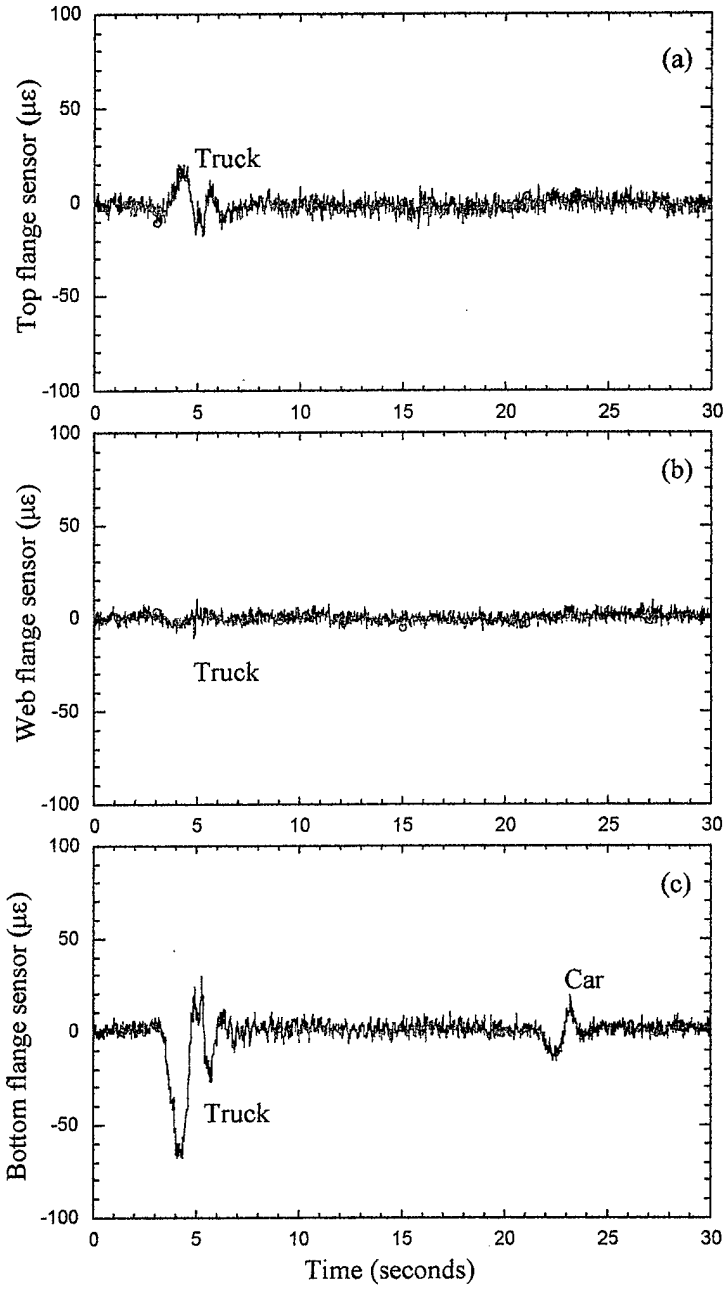

Figure 15 Response due to transient loading from FBG sensors located at (a) the topflange, (b) the web and (c) the bottom flange of the 1/8-spand, girder 3

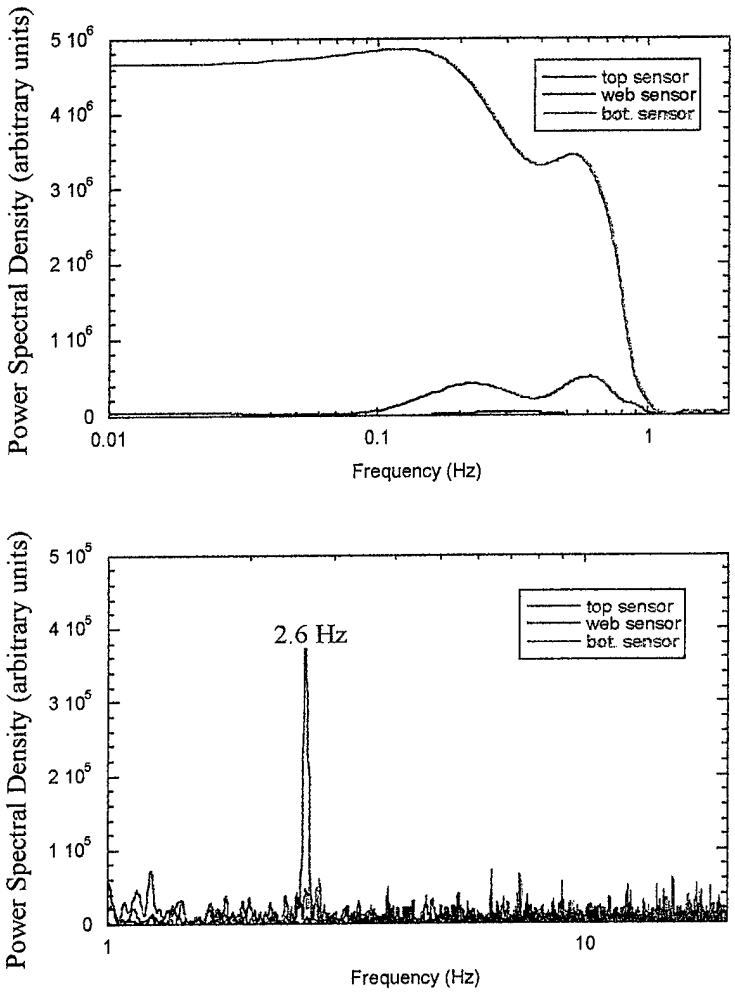

Figure 16 Power spectral density (in arbitrary amplitude units) of the top flange, bottom flange and the web FBG sensors located at girder 3, 1/8-span (see Fig. 15 for corresponding time series). The top part of the figure, (a) shows the power spectra of the data corresponding to the first 8 seconds of the time series while (b) corresponds to the power spectra of the time series from 8 to 30 seconds.

CONCLUSIONS

We have presented preliminary strain measurements performed on an in-operation bridge (I-10, New Mexico) using fiber Bragg grating sensors. The 32-channel system showed wide range of peak strains being induced at various locations on the girders of the bridge structure. These measurements show that it is possible to not only distinguish between heavy (e.g. trucks) and light (e.g. cars) transient loading events occurring on the bridge but it is also possible to determine the induced bridge vibrations. The measurements also imply that more advanced data processing techniques (e.g. wavelet analysis or wave propagation techniques) should be applied to the data obtained from spatially distributed arrays of sensors. The tests conducted so far demonstrate that FBG strain sensing systems are well suited for infra-structure health monitoring.

REFERENCES

1. A.D. Kersey, M.A. Davis, H.J. Patrick, M. LeBlanc, K.P. Koo, C.G. Askins, M.A. Putnam and E.J. Frieble, J. Lightwave Technol., Vol. 15, p. 1442 (1997).
2. A. D. Kersey et.al., Optics Letters, Vol. 18, p. 1370 (1993).